# Mind the Context: Attention-Guided Weak-to-Strong Consistency for Enhanced Semi-Supervised Medical Image Segmentation

Yuxuan Cheng<sup>1†</sup>, Chenxi Shao<sup>1†</sup>, Jie Ma<sup>1</sup>, and Guoliang Li<sup>1,2\*</sup>

Huazhong Agricultural University, Wuhan430070, China {hxwxss,alicespring,margo820}@webmail.hzau.edu.cn guoliang.li@mail.hzau.edu.cn

National Key Laboratory of Crop Genetic Improvement, Hubei Hongshan Laboratory, Agricultural Bioinformatics Key Laboratory of Hubei Province, Hubei Engineering Technology Research Center of Agricultural Big Data, Key Laboratory of Smart Farming Technology for Agricultural Animals, 3D Genomics Research Center, Huazhong Agricultural University, Wuhan430070, China

Abstract. Medical image segmentation is a pivotal step in diagnostic and therapeutic processes, relying on high-quality annotated data that is often challenging and costly to obtain. Semi-supervised learning offers a promising approach to enhance model performance by leveraging unlabeled data. Although weak-to-strong consistency is a prevalent method in semi-supervised image segmentation, there is a scarcity of research on perturbation strategies specifically tailored for semi-supervised medical image segmentation tasks. To address this challenge, this paper introduces a simple yet efficient semisupervised learning framework named Attention-Guided weak-to-strong Consistency Match (AIGC-Match). The AIGCMatch framework incorporates attention-guided perturbation strategies at both the image and feature levels to achieve weak-to-strong consistency regularization. This method not only preserves the structural information of medical images but also enhances the model's ability to process complex semantic information. Extensive experiments conducted on the ACDC and ISIC-2017 datasets have validated the effectiveness of AIGCMatch. Our method achieved a 90.4% Dice score in the 7-case scenario on the ACDC dataset, surpassing the state-of-the-art methods and demonstrating its potential and efficacy in clinical settings. Additionally, on the ISIC-2017 dataset, we significantly outperformed our baseline, indicating the robustness and generalizability of AIGCMatch across different medical image segmentation tasks.

Keywords: Weak-to-Strong Consistency · Medical Image Segmentation · Semi-Supervised Learning.

<sup>†</sup> Equal contribution. \*Corresponding author.

#### 1 Introduction

Medical image segmentation is a fundamental task aimed at delineating anatomical structures such as organs and tumors by classifying each pixel into distinct categories [32,17]. The precision achieved through medical image segmentation provides invaluable volumetric and shape details, serving as foundational elements for disease diagnosis, treatment efficacy evaluation, and quantitative analysis within clinical settings[9,24,14]. Data-driven approaches, particularly those based on fully supervised learning, have shown remarkable performance in this domain [26,8,22]. However, their success relies heavily on the availability of large-scale, high-quality annotated datasets, which are often challenging and expensive to obtain [31,17]. This limitation has spurred the development of semi-supervised learning (SSL) approaches, which leverage abundant unannotated data alongside a smaller set of annotated examples [23,39].

In the domain of SSL, consistency regularization has emerged as a key technique to use unannotated data to improve model performance [23,5,16,20,33,45]. The principle behind consistency regularization requires the model to produce consistent predictions on different perturbations of the input data. This is particularly relevant in medical imaging, where slight variations in image acquisition parameters or patient positioning can lead to variations in the appearance of the same anatomical structures [17]. Despite the remarkable performance of consistency Regularization, a critical limitation in current methods is their reliance on random perturbations to simulate data variability [37]. This approach, while effective for natural images with clear foreground-background distinctions, may not fully capture the complex high-dimensional semantic information of medical images. For example, in Fig 1, a model can easily segment a cat from the background in a scene because of the significant variation in pixels. However, segmenting organs or tissues from images not only requires the injection of proprietary semantic information but there are no clear pixel differences between different categories. This discrepancy between the natural images and the medical images calls for a specialized perturbation strategy tailored for semi-supervised medical image segmentation, a gap that existing works have yet to adequately address.

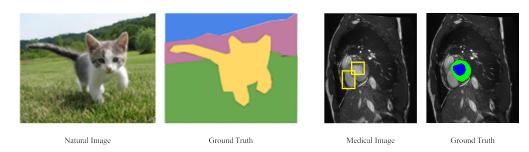


**Fig. 1.** An example of the difference between a natural image and medical image. In natural images, there is a clear pixel-level difference between the foreground, such as a cat, and the background, such as grassland. In contrast, within medical imaging, the two parts enclosed by the yellow boxes do not exhibit significant pixel-level differences; however, they represent semantically distinct entities.

This realization has catalyzed the development of our novel framework, AttentIon -Guided Consistency regularization Match (AIGCMatch), which rethinks the perturbation process. The framework shifts the focus from random perturbations to attention-guided perturbations. By harnessing the power of attention mechanisms, our method rethinks the notions of strong and weak consistency regularization at both the image and feature levels. At the feature level, our method leverages the skip connection structure of the U-net, utilizing the channel attention mechanism generated by the encoder layers to identify important channels within the feature maps. We introduce noise into these salient channels, as well as into less significant ones, allowing the features with perturbation to be passed along to the corresponding decoder layers through the U-net's skip connections. This process enables the model to supervise the predictions from the noised important channels input using the predictions from the noised unimportant channels input. The method of consistency regularization at the feature level is called AttFeaPerb in our paper. At the image level, we depart from previous consistency regularization methods that employed random perturbation techniques such as CutMix [38]. Instead, we utilize the model's attention map to identify key regions within the image for targeted CutMix as a strong perturbation named attention-guided CutMix (AttCutMix). We

then use weak perturbations at the image level to supervise the predictions from the input. In summary, unlike random perturbations, attention-guided perturbations have two advantages: 1) At the image level, attention-guided CutMix perturbs semantically related areas as a whole, maintaining the perturbation intensity without destroying the structural information of medical images. 2) At the feature level, perturbing by selecting channels with high attention is conducive to generating stronger perturbations to the model, promoting more robust model predictions. Our contributions are summarised as follows:

- We present a simple yet efficient semi-supervised framework named **AIGCMatch** for the practical medical image segmentation problem by taking advantage of a large amount of unlabeled data, which largely reduces annotation efforts for cardiac surgeons.
- We explore an effective perturbation strategy that uses the model's own attention to guide perturbations at image and feature levels.
- Through extensive experimentation on the ACDA dataset, we validate the efficacy of **AIGCMatch**. Our framework consistently outperforms state-of-the-art methods, demonstrating its effectiveness and potential for widespread adoption in clinical settings.

#### 2 Related Work

#### 2.1 Medical Image Analysis

Medical image analysis is crucial for computer-aided diagnosis and treatment planning, with applications in identifying pathological tissues and tracking disease progression [12]. Advances in imaging modalities like CT, MRI, and US have significantly enhanced the visualization of internal structures. A pivotal task in this field is medical image segmentation, which aids in precise diagnoses and planning by delineating regions of interest. The advent of deep learning, particularly Encoder-Decoder architectures, has revolutionized medical image segmentation. Early network design breakthroughs included the U-Net [26], which introduced a symmetric encoder-decoder structure and skip connections, setting new standards for accuracy and efficiency. Building on U-Net's success, variants like U-Net++ [44] and U-Net3+ [10] were proposed to improve feature fusion and segmentation performance with additional enhancements. The emergence of the Visual Transformer (ViT) model has led to hybrid architectures combining CNNs for local spatial information and Transformers for long-range dependencies and semantic processing [41,34,21].

#### 2.2 Semi-supervised medical image segmentation

However, medical image segmentation based fully supervised are heavily dependent on large volumes of expert-annotated data, which is a time-consuming, labor-intensive, and expensive process [15]. Additionally, these models may suffer from reduced effectiveness when encountering novel data or shifts in data distribution, thereby constraining their generalizability[16]. To address the above-mentioned question, researchers have introduced semi-supervised learning into medical image segmentation. Previous methods of semi-supervised medical image segmentation rely on the combination of a limited amount of labeled data and a vast quantity of unlabeled data to enhance model performance. These methods primarily include pseudo-labeling, graphical models, generative models, and autoencoders.

Pseudo-labeling involves utilizing predictions from a model trained on labeled data to generate pseudo-labels for unlabeled data. These pseudo-labels are then used to augment the training set and train the model iteratively [40,35,19]. Graphical model approaches to leverage the structure of graphs to represent pixel relationships within images, maximizing the posterior probability of labeled data for segmentation [29,1,6]. As highlighted by Litjens et al. [17], these methods typically construct an energy function that models the relationships between pixel labels and neighboring pixels, promoting label consistency within similar regions. Although these approaches perform well on small-scale datasets, they often face computational complexity and a lack of labeled information when applied to large-scale imaging data. Generative models, particularly Generative Adversarial Networks (GANs), have also gained widespread application in semi-supervised medical image segmentation [30,13,11]. Ouali et al. [25] note that GANs, through the adversarial training of generators and discriminators, not only generate realistic samples but also effectively leverage unlabeled data. This capability enables models to achieve improved segmentation performance with limited labeled samples.

#### 4 Y. Cheng et al.

**Autoencoder** is another commonly used method in semi-supervised learning[7,27,28], which compresses input images into lower-dimensional representations and then reconstructs the original images. As mentioned by Sajjadi et al. [27], through self-supervised learning on unlabeled data, autoencoders can extract important features that provide richer information for segmentation tasks.

While these previous methods laid the foundation for subsequent techniques, they still encounter challenges in dealing with imbalanced data and noise in complex scenarios.

# 2.3 Applications of Consistency Regularization and Weak-to-Strong Consistency in Semi-Supervised Medical Image segementation

Consistency regularization[5,3,20] serves as an effective semi-supervised learning strategy that enhances the robustness of models to input perturbations, thus advancing medical image segmentation. According to Xie et al.[36], this strategy ensures that the model's predictions remain consistent across various transformations of the input data, thereby improving generalization and providing new perspectives for the effective utilization of unlabeled data.

In practical applications, strong consistency and weak consistency are two essential components of consistency regularization, each playing a distinct role. Strong consistency mandates that the model maintains output consistency under significant transformations, such as rotation, scaling, or color changes. This strategy aids in enhancing the model's stability in complex scenarios, ensuring that it can still make accurate predictions in the face of real-world variations. Research by Ouali et al.[25] indicates that imposing strong consistency constraints can significantly improve model performance on complex medical images.

In contrast, weak consistency focuses on maintaining prediction consistency under minor perturbations, such as low noise levels or slight geometric changes. Sajjadi et al.[27] emphasize that this strategy effectively captures subtle structural variations, making it particularly suitable for complex biomedical images. Weak consistency not only enhances the model's resistance to noise but also improves segmentation accuracy, rendering semi-supervised learning more practical in medical image segmentation tasks.

In previous works, the effectiveness of strong consistency and weak consistency in image segmentation has been well established. However, when it comes to weak-to-strong consistency, applications of this simple yet effective method in the field of medical imaging remain relatively scarce. Yang et al. proposed Unimatch [37], a novel framework for semi-supervised image segmentation based on weak-to-strong consistency, which achieved state-of-the-art performance across various datasets, including the ACDC dataset. This achievement highlights the potential of strong and weak consistency in semi-supervised medical image segmentation and has inspired a series of subsequent works, such as CrossMatch[42]. Inspired by previous work, we propose an attention-guided perturbation approach that emphasizes contextual information in medical images and improves the ability of models for semi-supervised medical image segmentation.

### 3 Method

#### 3.1 The Overview of Framework

As depicted in Fig2, the proposed framework consists of two attention-guided perturbation modules in image and feature level, aiming to enhance the capability of the semi-supervised segmentation model to capture complex structural and high-dimensional semantic information in medical images. To enhance the pertinence of perturbations to the model, we fully leverage the attention from various parts of the model. At each level, the perturbations are crafted according to the attention derived from the respective parts of the model. In Fig 3, we compared the differences between our model and the Unimatch[37]. It comprises a supervised branch and two unsupervised branches. The model is supervised for labeled data by computing the loss between the model's predictions and the ground truth (GT). For unlabeled data, attention maps from the model are employed to guide perturbations at both the feature and the image levels. Specifically, at the feature level, we proposed AttFeaPerb to obtain strong perturbation predictions  $p^{fsp} \in \mathbb{R}^{C \times H \times W}$  and weak perturbation predictions  $p^{fwp} \in \mathbb{R}^{C \times H \times W}$ . At the image level, we used predictions  $p^{w} \in \mathbb{R}^{C \times H \times W}$  obtained from weak perturbations to supervise the predictions  $p^{s1} \in \mathbb{R}^{C \times H \times W}$  and  $p^{s2} \in \mathbb{R}^{C \times H \times W}$  obtained from AttCutMix.

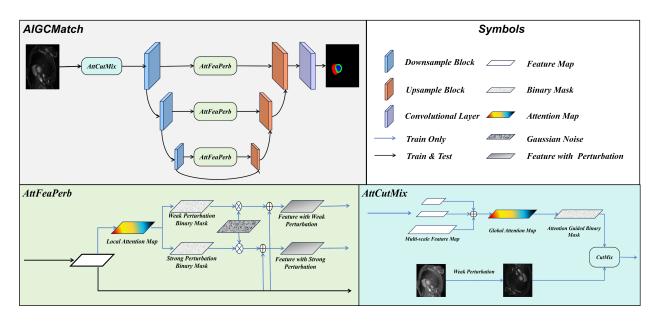


Fig. 2. Our proposed method, AIGCMatch. Labeled data ignores the perturbation for supervised training. As for unlabeled data, we use AttCutMix for image perturbation and AttFeaPerb for feature perturbation to self-supervised training.

#### 3.2 Attention-Guided Perturbation in Image Level

In previous studies, randomization methods such as CutMix have been the most common approach to introduce strong perturbations at the image level in semi-supervised image segmentation. However, these methods do not consider the actual semantics of the cropped content [18], which can disrupt contextual and semantic information within the image and weaken the model's ability to extract deep-level image features.

Building upon the foundation of CutMix for the implementation of strong perturbations at the image level, we introduce a variant termed Attention-guided CutMix (AttCutMix). This method leverages the model's attention mechanism to identify and select regions within the training image that exhibit heightened attention scores. These regions are then strategically swapped with corresponding segments from other images, thereby synthesizing novel training data that can be utilized for unsupervised training phases within our model's regimen.

To describe the Attention-guided CutMix method (AttCutMix), let  $x \in \mathbb{R}^{C \times H \times W}$  represent the input image, and let  $y \in \mathbb{R}^{H \times W}$  represent the model's prediction for the input image.  $(x_A, y_A)$  and  $(x_B, y_B)$  represent two different sets of unlabeled training data together with the predictions of the model for these inputs. $(\hat{x}, \hat{y})$  represents the new training data synthesized by the AttCutMix method. The operation of AttCutMix can be formalized through the following set of equations:

$$M = A_{decoder} > \gamma \tag{1}$$

$$\hat{x} = M \odot x_A + (1 - M) \odot x_B \tag{2}$$

$$\hat{y} = M \odot y_A + (1 - M) \odot y_B \tag{3}$$

where  $A_{decoder}$  refers to the attention map output by the model's decoder component,  $\gamma$  denotes a pre-defined hyperparameter that is instrumental in controlling the generation of a binary matrix. Specifically, M is a binary matrix denoted as  $M \in \{0,1\}^{H \times W}$ , which means the regions of the image that are designated for exchange. By fine-tuning the hyperparameter, the objective of AttCutMix is to ensure the preservation of semantic information in the salient parts of the image, while simultaneously introducing beneficial perturbations. In addition to this, we have adopted the Dual-stream Perturbation approach from Unimatch, utilizing AttCutMix to generate two distinct strongly perturbed images for unsupervised training.

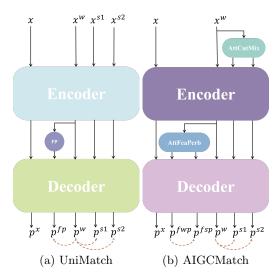


Fig. 3. Comparison with UniMatch and AIGCMatch. (a)The UniMatch baseline. The Fp denotes feature perturbation. (b) Our proposed AIGCMatch. AttCutMix denotes our method of image perturbation, while AttFeaPerb denotes our method of feature perturbation, and the dashed curves represent supervision.

#### 3.3 Exploring Weak-to-Strong Consistency in the Feature Level

In previous studies, discussions and definitions regarding the consistency of weak and strong perturbations have been confined to disturbances at the image level. Disturbances such as image rotation, translation, and scaling have been categorized as weak perturbations, while color transformations and CutMix operations have been defined as strong perturbations. However, no clear distinction has been made between weak and strong perturbations at the feature level.

Inspired by the concept of weak and strong consistency at the image level, we propose the notion of weak-to-strong consistency regularization at the feature level. In the context of feature-level perturbations, we define the addition of a perturbation to channels with lower attention within the model as a weak perturbation operation. Conversely, adding perturbation to channels with higher attention within the model is a strong perturbation operation. Empirical evidence suggests that the quality of the model's predictive outcomes for features subjected to weak perturbations is superior to those for features experiencing strong perturbations. Consequently, during the model training process, we utilize the model's predictions on weakly perturbed features to supervise the predictions of strongly perturbed features, which we call attention-guided feature perturbation (AttFeaPerb).

For perturbations at the feature level, we introduce noise to the feature maps corresponding to each downsampling module of the model encoder based on the attention given to the image by that module. These perturbed feature maps are then conveyed to the upsampling modules of the corresponding decoder through the skip connection architecture of the U-Net. To reduce the learning difficulty for the model, we gradually increase the intensity of the feature-level perturbation by the number of training epochs.

We define  $F_i \in \mathbb{R}^{C_i H_i W_i}$  as the feature map of the *i*-th downsampling module in the encoder.  $F_i^w \in \mathbb{R}^{C_i H_i W_i}$  represents the characteristic vector of the *i*-th downsampling module after applying weak perturbation.  $F_i^S \in \mathbb{R}^{C_i H_i W_i}$  denotes the feature vector of the *i*-th downsampling module following the application of strong perturbation.  $A_i \in \mathbb{R}^{H_i W_i}$  signifies the heatmap of the *i*-th downsampling module. The operations for perturbation at the feature level can be expressed with the following formulas:

$$M_i = A_i > \beta \tag{4}$$

$$F_i^W = F_i + G(F_i) \odot (t(x) \times M_i)$$
(5)

$$F_i^S = F_i + G(F_i) \odot (t(x) \times (1 - M_i) + \phi)$$

$$\tag{6}$$

where  $\beta$  is a pre-defined hyperparameter utilized for controlling the generation of matrix  $M_i$ , The matrix  $M_i \in \{0,1\}^{H \times W}$  is a binary matrix indicating which locations in the feature map should be perturbed.  $G(F_i)$  is a Gaussian noise generation function designed to produce a Gaussian noise matrix of the same shape as

 $F_i$ . t(x) is a monotonically increasing function that controls the intensity of the perturbation, and  $\phi$  is a bias term. Specifically, the function t(x) can be represented in the following form:

$$t(x) = 1 - k \times (1 - \frac{x}{epoch})^{0.9} \tag{7}$$

In the above equation, k is a pre-defined hyperparameter that represents the maximum intensity of the perturbation to be added. x denotes the current epoch number during training, and epoch signifies the total number of training epochs.

#### 3.4 Loss Function

In semi-supervised image segmentation tasks, the loss function typically consists of two components: supervised loss and unsupervised loss. We denote the loss function as  $\mathcal{L}$ , the supervised loss as  $\mathcal{L}_x$ , and the unsupervised loss as  $\mathcal{L}_u$ . The final loss function can be formally expressed as:

$$\mathcal{L} = \frac{1}{2}(\mathcal{L}_x + \mathcal{L}_u) \tag{8}$$

For the supervised loss, we employ both cross-entropy loss and Dice coefficient loss. As for the unsupervised loss, it is divided into two parts: the loss for image-level consistency  $\mathcal{L}_s$  and the loss for feature-level consistency  $\mathcal{L}_{fp}$ .

We define  $x^w \in \mathbb{R}^{C \times H \times R}$  as the weakly perturbed unlabeled training data generated.  $x^{s_1} \in \mathbb{R}^{C \times H \times W}$ ,  $x^{s_2} \in \mathbb{R}^{C \times H \times W}$  represent the two sets of strongly perturbed unlabeled training data generated.  $p^w \in \mathbb{R}^{H \times W}$ ,  $p^{s_1} \in \mathbb{R}^{H \times W}$ ,  $p^{s_2} \in \mathbb{R}^{H \times W}$  denote the model predictions for the unlabeled training data with different levels of perturbation, respectively. We define the image consistency loss function  $\mathcal{L}_s$  as follows:

$$\mathcal{L}_s = \frac{1}{B_u} \sum \mathbb{1} \left( \max(p^w) \ge \tau \right) \cdot \left( H(p^w, p^{s_1}) + H(p^w, p^{s_2}) \right)$$
 (9)

In the above equation,  $B_u$  represents the batch size of the unlabeled data,  $\tau$  is a pre-set confidence threshold used to mitigate the impact of noise on model training, and H calculates the entropy distance between two sets of predictions.

For the loss of feature-level consistency between strong and weak perturbations  $\mathcal{L}_{fp}$ , we define  $p^{fsp} \in \mathbb{R}^{H \times W}$ ,  $p^{fwp} \in \mathbb{R}^{H \times W}$  to represent the model's predictive outcomes after applying strong and weak perturbations to the features, respectively. We define the loss function for feature consistency  $\mathcal{L}_{fp}$  as follows:

$$\mathcal{L}_{fp} = \frac{1}{B_u} \sum \mathbb{1} \left( \max(p^{fwp}) \ge \tau \right) \cdot \mathcal{H}(p^{fwp}, p^{fsp})$$
 (10)

Hereby, we can articulate the expression for the unsupervised loss function as follows:

$$\mathcal{L}_{u} = \frac{1}{B_{u}} \sum \mathbb{1} \left( \max(p^{w}) \ge \tau \right) \cdot \left( \frac{\lambda}{2} \left( \mathbf{H}(p^{w}, p^{s_{1}}) \right) + \mathbf{H}(p^{w}, p^{s_{2}}) \right) + \mathbb{1} \left( \max(p^{fwp}) \ge \tau \right) \cdot \left( \mu \mathbf{H}(p^{fwp}, p^{fsp}) \right)$$

$$(11)$$

The weights for the loss function, denoted as  $\lambda$  and  $\mu$ , are set to 0.5. In the unsupervised loss  $L_u$ , the function H is commonly used as the Dice coefficient loss.

### 4 Experiments

#### 4.1 Experimental Setups

**Datasets** In this research, we evaluated our model's performance on the ACDC and ISIC-2017 within a semi-supervised learning framework for medical image segmentation. The ACDC dataset[4], consisting of 100 two-dimensional cine cardiac MR images from the University Hospital of Dijon, is divided into 70 scans for training, 10 for validation, and 20 for testing. It is unique in targeting multiclass segmentation of cardiac

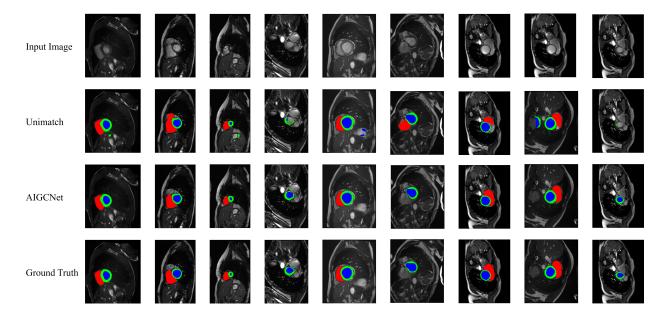


**Fig. 4.** Comparison with ground truth and two different results. Three different colors depicted in the figure represent three distinct segmentation outcomes. The section enclosed in a light blue box indicates areas where the model has either made an erroneous prediction or has omitted a prediction.

structures, contrasting with other datasets that focus on binary segmentation. Within the domain of semi-supervised medical image segmentation, the ACDC dataset is conventionally divided into distinct segments categorized as 1-case, 3-case, and 7-case. These categories correspond to the utilization of 1%, 5%, and 10% of the available labeled data, respectively.

For the ISIC-2017 dataset, we adopted a similar semi-supervised learning strategy. This dataset, which encompasses a wide range of skin lesion images, is an excellent resource for evaluating segmentation models in the context of dermatology. We utilized 10% of the labeled images for training, which amounts to 200 images, and the remaining 90% as unlabeled data for our semi-supervised model. The validation set within ISIC-2017 contains 150 images, which were used to evaluate the model's performance in a real-world scenario.

Implementation Details To ensure a fair comparison with prior work, we have adopted the U-Net architecture as the backbone for our segmentation model. Following previous work [37,2], we employ the Dice Similarity Coefficient (DSC), the Jaccard Index, the 95th percentile Hausdorff Distance (95HD), and the Average Surface Distance (ASD) to evaluate the segmentation accuracy of our medical image analysis model. During the training process, each batch consists of an equal mix of 12 labeled and 12 unlabeled data samples. We initialized the learning rate at 0.01 and used an SGD optimizer. The model was trained for 300 epochs under a learning rate scheduler. The original images were resized to vary between 0.5 and 2.0 times their original dimensions, and subjected to cropping and flipping to obtain their weakly perturbed versions.

## 4.2 Semi-supervised image segmentation in ACDC

In the ACDC dataset, we compared our experimental results with those of multiple models, consistently achieving superior results. In comparison to the previous state-of-the-art (SOTA), our method demonstrated improvements across four metrics: DICE, Jaccard, 95HD, and ASD.

It should be noted that, compared to previous methodologies, our approach has yielded outcomes equivalent or superior to those of other models that have used 10% labeled data, although it only employs 5% labeled data. Furthermore, compared to previous methods that labeled 5% labeled data, our approach has achieved comparable or superior outcomes with only 1% of the data, which has often been overlooked due to their poor performance in previous studies. This substantiates the superior performance and substantial potential of AIGCMatch in the domain of medical image segmentation.

Method	1 case	3 case	7 case	
	DICE $\uparrow$ / Jaccard $\uparrow$ / 95HD $\downarrow$ / ASD $\downarrow$			
SupBaseline	28.50/16.62/ - / -	47.83/37.01/31.16/12.62	79.41/68.11/9.35/2.70	
UA-MT (MICCAI 2019)	- / - / - / -	46.04/35.97/20.08/7.75	81.65/70.64/6.88/2.02	
DTC (AAAI 2021)	- / - / - / -	$56.90/45.67/\ 23.36/7.39$	84.29/73.92/12.81/4.01	
SS-Net(MICCAI 2022)	- / - / - / -	65.82/55.38/6.67/2.28	86.78/77.67/6.07/1.40	
BCP (CVPR 2023)	- / - / - / -	87.59/78.67/1.90/0.67	88.84/80.62/ 3.98/1.17	
Unimatch (CVPR 2023)	85.43/74.57/ - / -	88.86/ 79.95 / - / -	89.85/81.57/-/-	
CrossMatch(Arxiv 2024)	- / - / - / -	88.27/80.17/1.53/0.46	89.08/81.44/1.52/0.52	
Ours	$86.25 \pm 2.50 / 75.82 / 1.11 / 0.21$	$89.53 \pm 2.15 / 81.07 / 0.94 / 0.17$	$90.40 \pm 1.68 / 82.48 / 0.86 / 0.14$	

**Table 1.** Comparison with seven different models on the ACDC dataset, using 1, 3, and 7 labeled cases. SupBaseline denotes the performance achieved by supervised leveraging solely labeled imagery within the scope of the study. Our method, AIGCMatch, has the best performance.

#### 4.3 Semi-supervised image segmentation in ISIC-2017

The ISIC-2017 dataset is widely recognized as challenging[43], In our research, we conducted a thorough performance comparison on the ISIC-2017 dataset, evaluating our method against a baseline model. As illustrated in Table 2, the Weak-to-Strong Consistency-based Random Perturbation method (Unimatch) exhibited inferior performance compared to the Supervised Baseline (SupBaseline).

Method	DICE(%) ↑	$Jaccard(\%) \uparrow$
SupBaseline	73.74	58.4
Unimatch(baseline model)	68.92	52.57
Ours	74.58	<b>59.46</b>

Table 2. Comparison with baseline on the ISIC-2017 dataset, using 10% labeled data. SupBaseline denotes the performance achieved by supervised leveraging solely labeled imagery within the scope of the study. Our method, AIGCMatch, has the best performance.

In contrast, our approach demonstrated a substantial improvement over Unimatch, achieving notable advancements over the SupBaseline. Specifically, our method outperformed the supervised baseline by 0.84% in terms of the Dice Similarity Coefficient and by 1.06% in the Jaccard index. These results indicate the effectiveness of our method in enhancing segmentation performance on the ISIC-2017 dataset, suggesting its potential for broader applications in medical image analysis.

#### 4.4 Ablation study

To rigorously assess the effectiveness of each component within our framework, we have meticulously designed and executed a series of systematic experiments. These experiments isolate and evaluate the impact of individual elements within the framework.

Ablation study on Perturbation at the image and feature level Primarily, we aim to establish the validity of the attention-guided perturbation at both the image and feature levels. To achieve this, we introduce the attention-guided perturbation at various levels of the model and compare its performance with the introduction of random noise, a technique employed by UniMatch.

Image perturbation	Feature perturbation	MeanDice (%)
Random	Random	89.85
Random	AttFeaPerb	90.20
AttCutMix	Random	89.92
$\mathbf{AttCutMix}$	$\mathbf{AttFeaPerb}$	90.40

**Table 3.** Comparison with 4 different methods to add perturbation. Random represents adding perturbation randomly while AttPerb represents the attention-guided perturbation method.

Based on the findings presented in Table 3, it can be observed that the utilization of attention-guided perturbation strategies leads to enhancements in model performance, irrespective of whether the perturbation is applied simultaneously at the image level, the feature level, or across both levels.

Ablation study on Perturbation methods To substantiate the efficacy of AttCutMix and AttFeaPerb, we conducted 4 sets of experiments on the ACDC dataset under three distinct partition schemes: 1 case, 3 cases, and 7 cases. The methodologies used in these experiments were the Baseline, the AttCutMix strategy, the AttFeaPerb strategy, and AIGCMatch, respectively.

Method	1 case	3 cases	7 cases
Baseline	85.43	88.86	89.85
Baseline AttCutMix AttFeaPerb AIGCMatch	86.56	89.13	89.92
AttFeaPerb	85.23	89.25	90.20
AIGCMatch	86.25	89.53	90.40

Table 4. Comparison with 4 different methodologies on the ACDC dataset, using 1, 3, and 7 labeled cases.

Examination of Table 4 reveals that AttCutMix and AttFeaPerb have improved over the original model across experiments with varying proportions of labeled data. Furthermore, integrating these two methods, AIGCMatch has resulted in state-of-the-art performance.

#### 5 Conclusions

In this study, we introduced an easy yet efficient semi-supervised segmentation framework termed Attention-Guided weak-to-strong Consistency Match (AIGCMatch), aiming at enhancing the performance of medical image segmentation. By employing attention-guided perturbation strategies at both the image and feature levels, AIGCMatch achieves weak-to-strong consistency and preserves the structural information of medical images as well. Experiments on the ACDC dataset and ISIC-2017 dataset demonstrate the effectiveness of our approach, and we achieve the performance of SOTA on the ACDC dataset. Our work demonstrates the efficacy of attention-guided perturbation strategies in medical image segmentation, improving model robustness by introducing structured and semantically relevant perturbations within the model's decision-making process.

However, there is still room for further improvement and expansion. Future work will explore the application of AIGCMatch to a broader range of medical image datasets and investigate its performance on more complex and diverse medical images.

#### References

- Alansary, A., Kamnitsas, K., Davidson, A., Khlebnikov, R., Rajchl, M., Malamateniou, C., Rutherford, M., Hajnal, J.V., Glocker, B., Rueckert, D., et al.: Fast fully automatic segmentation of the human placenta from motion corrupted mri. In: Medical Image Computing and Computer-Assisted Intervention-MICCAI 2016: 19th International Conference, Athens, Greece, October 17-21, 2016, Proceedings, Part II 19. pp. 589-597. Springer (2016)
- Bai, Y., Chen, D., Li, Q., Shen, W., Wang, Y.: Bidirectional copy-paste for semi-supervised medical image segmentation. In: Proceedings of the IEEE/CVF Conference on Computer Vision and Pattern Recognition (CVPR). pp. 11514–11524 (June 2023)
- Basak, H., Bhattacharya, R., Hussain, R., Chatterjee, A.: An exceedingly simple consistency regularization method for semi-supervised medical image segmentation. In: 2022 IEEE 19th International Symposium on Biomedical Imaging (ISBI). pp. 1–4. IEEE (2022)
- 4. Bernard, O., Lalande, A., Zotti, C., Cervenansky, F., Yang, X., Heng, P.A., Cetin, I., Lekadir, K., Camara, O., Gonzalez Ballester, M.A., Sanroma, G., Napel, S., Petersen, S., Tziritas, G., Grinias, E., Khened, M., Kollerathu, V.A., Krishnamurthi, G., Rohé, M.M., Pennec, X., Sermesant, M., Isensee, F., Jäger, P., Maier-Hein, K.H., Full, P.M., Wolf, I., Engelhardt, S., Baumgartner, C.F., Koch, L.M., Wolterink, J.M., Išgum, I., Jang, Y., Hong, Y., Patravali, J., Jain, S., Humbert, O., Jodoin, P.M.: Deep learning techniques for automatic mri cardiac multi-structures segmentation and diagnosis: Is the problem solved? IEEE Transactions on Medical Imaging 37(11), 2514–2525 (2018). https://doi.org/10.1109/TMI.2018.2837502
- Bortsova, G., Dubost, F., Hogeweg, L., Katramados, I., De Bruijne, M.: Semi-supervised medical image segmentation via learning consistency under transformations. In: Medical Image Computing and Computer Assisted Intervention–MICCAI 2019: 22nd International Conference, Shenzhen, China, October 13–17, 2019, Proceedings, Part VI 22. pp. 810–818. Springer (2019)
- Cai, J., Lu, L., Zhang, Z., Xing, F., Yang, L., Yin, Q.: Pancreas segmentation in mri using graph-based decision fusion on convolutional neural networks. In: International Conference on Medical Image Computing and Computer-Assisted Intervention. pp. 442–450. Springer (2016)
- Chen, S., Bortsova, G., García-Uceda Juárez, A., Van Tulder, G., De Bruijne, M.: Multi-task attention-based semi-supervised learning for medical image segmentation. In: Medical Image Computing and Computer Assisted Intervention-MICCAI 2019: 22nd International Conference, Shenzhen, China, October 13–17, 2019, Proceedings, Part III 22. pp. 457–465. Springer (2019)
- 8. Çiçek, Ö., Abdulkadir, A., Lienkamp, S.S., Brox, T., Ronneberger, O.: 3d u-net: learning dense volumetric segmentation from sparse annotation. In: Medical Image Computing and Computer-Assisted Intervention-MICCAI 2016: 19th International Conference, Athens, Greece, October 17-21, 2016, Proceedings, Part II 19. pp. 424–432. Springer (2016)
- 9. Heller, N., Isensee, F., Maier-Hein, K.H., Hou, X., Xie, C., Li, F., Nan, Y., Mu, G., Lin, Z., Han, M., et al.: The state of the art in kidney and kidney tumor segmentation in contrast-enhanced ct imaging: Results of the kits19 challenge. Medical image analysis 67, 101821 (2021)
- 10. Huang, H., Lin, L., Tong, R., Hu, H., Zhang, Q., Iwamoto, Y., Han, X., Chen, Y.W., Wu, J.: Unet 3+: A full-scale connected unet for medical image segmentation. In: ICASSP 2020-2020 IEEE international conference on acoustics, speech and signal processing (ICASSP). pp. 1055–1059. IEEE (2020)
- 11. Hung, W.C., Tsai, Y.H., Liou, Y.T., Lin, Y.Y., Yang, M.H.: Adversarial learning for semi-supervised semantic segmentation. arXiv preprint arXiv:1802.07934 (2018)
- 12. Jiao, R., Zhang, Y., Ding, L., Xue, B., Zhang, J., Cai, R., Jin, C.: Learning with limited annotations: a survey on deep semi-supervised learning for medical image segmentation. Computers in Biology and Medicine p. 107840 (2023)
- 13. Laine, S., Aila, T.: Temporal ensembling for semi-supervised learning, arXiv preprint arXiv:1610.02242 (2016)
- Lalande, A., Chen, Z., Pommier, T., Decourselle, T., Qayyum, A., Salomon, M., Ginhac, D., Skandarani, Y., Boucher, A., Brahim, K., et al.: Deep learning methods for automatic evaluation of delayed enhancement-mri. the results of the emidec challenge. Medical Image Analysis 79, 102428 (2022)
- Leiner, T., Rueckert, D., Suinesiaputra, A., Baeßler, B., Nezafat, R., Išgum, I., Young, A.A.: Machine learning in cardiovascular magnetic resonance: basic concepts and applications. Journal of Cardiovascular Magnetic Resonance 21(1), 61 (2019)
- Li, X., Yu, L., Chen, H., Fu, C.W., Xing, L., Heng, P.A.: Transformation-consistent self-ensembling model for semisupervised medical image segmentation. IEEE transactions on neural networks and learning systems 32(2), 523–534 (2020)
- 17. Litjens, G., Kooi, T., Bejnordi, B.E., Setio, A.A.A., Ciompi, F., Ghafoorian, M., Van Der Laak, J.A., Van Ginneken, B., Sánchez, C.I.: A survey on deep learning in medical image analysis. Medical image analysis 42, 60–88 (2017)

- 18. Liu, J., Liu, B., Zhou, H., Li, H., Liu, Y.: Tokenmix: Rethinking image mixing for data augmentation in vision transformers. In: European Conference on Computer Vision. pp. 455–471. Springer (2022)
- 19. Lu, L., Yin, M., Fu, L., Yang, F.: Uncertainty-aware pseudo-label and consistency for semi-supervised medical image segmentation. Biomedical Signal Processing and Control 79, 104203 (2023)
- Luo, X., Chen, J., Song, T., Wang, G.: Semi-supervised medical image segmentation through dual-task consistency. In: Proceedings of the AAAI conference on artificial intelligence. vol. 35, pp. 8801–8809 (2021)
- Manzari, O.N., Kaleybar, J.M., Saadat, H., Maleki, S.: Befunet: A hybrid cnn-transformer architecture for precise medical image segmentation. arXiv preprint arXiv:2402.08793 (2024)
- 22. Milletari, F., Navab, N., Ahmadi, S.A.: V-net: Fully convolutional neural networks for volumetric medical image segmentation. In: 2016 fourth international conference on 3D vision (3DV). pp. 565–571. Ieee (2016)
- 23. Oliver, A., Odena, A., Raffel, C., Cubuk, E., Goodfellow, I.: Realistic evaluation of semi-supervised learning algorithms. In: International conference on learning representations. pp. 1–15 (2018)
- 24. Oreiller, V., Andrearczyk, V., Jreige, M., Boughdad, S., Elhalawani, H., Castelli, J., Vallières, M., Zhu, S., Xie, J., Peng, Y., et al.: Head and neck tumor segmentation in pet/ct: the hecktor challenge. Medical image analysis 77, 102336 (2022)
- 25. Ouali, Y., Hudelot, C., Tami, M.: Semi-supervised semantic segmentation with cross-consistency training. In: Proceedings of the IEEE/CVF conference on computer vision and pattern recognition. pp. 12674–12684 (2020)
- Ronneberger, O., Fischer, P., Brox, T.: U-net: Convolutional networks for biomedical image segmentation. In: Medical image computing and computer-assisted intervention-MICCAI 2015: 18th international conference, Munich, Germany, October 5-9, 2015, proceedings, part III 18. pp. 234-241. Springer (2015)
- 27. Sajjadi, M., Javanmardi, M., Tasdizen, T.: Regularization with stochastic transformations and perturbations for deep semi-supervised learning. Advances in neural information processing systems 29 (2016)
- 28. Sedai, S., Mahapatra, D., Hewavitharanage, S., Maetschke, S., Garnavi, R.: Semi-supervised segmentation of optic cup in retinal fundus images using variational autoencoder. In: Medical Image Computing and Computer-Assisted Intervention- MICCAI 2017: 20th International Conference, Quebec City, QC, Canada, September 11-13, 2017, Proceedings, Part II 20. pp. 75–82. Springer (2017)
- 29. Shakeri, M., Tsogkas, S., Ferrante, E., Lippe, S., Kadoury, S., Paragios, N., Kokkinos, I.: Sub-cortical brain structure segmentation using f-cnn's. In: 2016 IEEE 13th international symposium on biomedical imaging (ISBI). pp. 269–272. IEEE (2016)
- 30. Souly, N., Spampinato, C., Shah, M.: Semi supervised semantic segmentation using generative adversarial network. In: Proceedings of the IEEE international conference on computer vision. pp. 5688–5696 (2017)
- 31. Tajbakhsh, N., Shin, J.Y., Gurudu, S.R., Hurst, R.T., Kendall, C.B., Gotway, M.B., Liang, J.: Convolutional neural networks for medical image analysis: Full training or fine tuning? IEEE transactions on medical imaging 35(5), 1299–1312 (2016)
- 32. Van Ginneken, B., Schaefer-Prokop, C.M., Prokop, M.: Computer-aided diagnosis: how to move from the laboratory to the clinic. Radiology **261**(3), 719–732 (2011)
- 33. Wang, Y., Zhang, Y., Tian, J., Zhong, C., Shi, Z., Zhang, Y., He, Z.: Double-uncertainty weighted method for semi-supervised learning. In: Medical Image Computing and Computer Assisted Intervention–MICCAI 2020: 23rd International Conference, Lima, Peru, October 4–8, 2020, Proceedings, Part I 23. pp. 542–551. Springer (2020)
- 34. Wang, Z., Min, X., Shi, F., Jin, R., Nawrin, S.S., Yu, I., Nagatomi, R.: Smeswin unet: Merging cnn and transformer for medical image segmentation. In: International Conference on Medical Image Computing and Computer-Assisted Intervention. pp. 517–526. Springer (2022)
- 35. Wu, H., Zhang, B., Chen, C., Qin, J.: Federated semi-supervised medical image segmentation via prototype-based pseudo-labeling and contrastive learning. IEEE Transactions on Medical Imaging 43(2), 649–661 (2024). https://doi.org/10.1109/TMI.2023.3314430
- 36. Xie, Q., Dai, Z., Hovy, E., Luong, T., Le, Q.: Unsupervised data augmentation for consistency training. Advances in neural information processing systems 33, 6256–6268 (2020)
- 37. Yang, L., Qi, L., Feng, L., Zhang, W., Shi, Y.: Revisiting weak-to-strong consistency in semi-supervised semantic segmentation. In: Proceedings of the IEEE/CVF Conference on Computer Vision and Pattern Recognition (CVPR). pp. 7236–7246 (June 2023)
- 38. Yun, S., Han, D., Oh, S.J., Chun, S., Choe, J., Yoo, Y.: Cutmix: Regularization strategy to train strong classifiers with localizable features. In: Proceedings of the IEEE/CVF international conference on computer vision. pp. 6023–6032 (2019)
- 39. Zhang, S., Zhang, J., Tian, B., Lukasiewicz, T., Xu, Z.: Multi-modal contrastive mutual learning and pseudo-label re-learning for semi-supervised medical image segmentation. Medical Image Analysis 83, 102656 (2023)
- 40. Zhang, W., Zhu, L., Hallinan, J., Zhang, S., Makmur, A., Cai, Q., Ooi, B.C.: Boostmis: Boosting medical image semi-supervised learning with adaptive pseudo labeling and informative active annotation. In: Proceedings of the IEEE/CVF conference on computer vision and pattern recognition. pp. 20666–20676 (2022)

- 41. Zhang, Y., Liu, H., Hu, Q.: Transfuse: Fusing transformers and cnns for medical image segmentation. In: Medical Image Computing and Computer Assisted Intervention-MICCAI 2021: 24th International Conference, Strasbourg, France, September 27-October 1, 2021, Proceedings, Part I 24. pp. 14-24. Springer (2021)
- 42. Zhao, B., Wang, C., Ding, S.: Crossmatch: Enhance semi-supervised medical image segmentation with perturbation strategies and knowledge distillation (2024), https://arxiv.org/abs/2405.00354
- 43. Zhou, Y., Huang, J., Wang, C., Song, L., Yang, G.: Xnet: Wavelet-based low and high frequency fusion networks for fully-and semi-supervised semantic segmentation of biomedical images. In: Proceedings of the IEEE/CVF International Conference on Computer Vision. pp. 21085–21096 (2023)
- 44. Zhou, Z., Rahman Siddiquee, M.M., Tajbakhsh, N., Liang, J.: Unet++: A nested u-net architecture for medical image segmentation. In: Deep Learning in Medical Image Analysis and Multimodal Learning for Clinical Decision Support: 4th International Workshop, DLMIA 2018, and 8th International Workshop, ML-CDS 2018, Held in Conjunction with MICCAI 2018, Granada, Spain, September 20, 2018, Proceedings 4. pp. 3–11. Springer (2018)
- 45. Zhu, Y., Zhang, Z., Wu, C., Zhang, Z., He, T., Zhang, H., Manmatha, R., Li, M., Smola, A.: Improving semantic segmentation via self-training, arxiv 2020, arXiv preprint arXiv:2004.14960 2 (2021)